Dual-Band Reconfigurable Graphene-Based Patch Antenna in Terahertz Band: Design, Analysis and Modeling Using WCIP Method

Aymen Hlali[*]**, Zied Houaneb, and Hassen Zairi**

Abstract—The resonant frequency of an antenna plays a crucial role in the design of a reconfigurable antenna. In this article, we have developed a dual-band reconfigurable terahertz patch antenna by using graphene. The simulation results demonstrate that the designed structure can provide excellent properties in terms of dual wide-band performance, frequency-reconfiguration by applying different voltages on the graphene. These initial results are particularly promising for various applications in the THz regime. Furthermore, we have investigated the effect of the additional parameter such as temperature and relaxation time. The modeling is done by using a new equation of the Wave Concept Iterative Process (WCIP) method, and the validation is achieved by comparison with CST simulator. Here, we propose to develop a new efficient and flexible numerical tool for graphene modeling.

1. INTRODUCTION

THz band is a portion of electromagnetic spectrum including frequencies in the range of 0.1 THz to 10 THz [1]. This band becomes extremely attractive due to essential properties such as the ability to pass through different materials with various levels of attenuation [2] and the abundance of bandwidth [3]. It has been used in numerous fields including spectroscopy, high-resolution radar, imaging and, more recently, wireless communications [4–7].

However, the THz regime is one of the ongoing challenges facing electronic and photonic materials and device engineering [8]. The solution to these developments is the exploration of the characteristics of new materials and devices at high frequencies. In search of efficient solutions to these problems, graphene appears as an excellent candidate for the implementation of new devices. Due to its unique properties at terahertz (THz) frequencies [9], graphene has attracted huge interests since it was successfully exfoliated in 2004 [10]. One of the most interesting properties of this material is its ability to support transverse magnetic surface plasmonic modes with unique properties. Specifically, graphene plasmons possess more confinement, low loss and good tunability via chemical or electrostatic gating at THz frequencies [11, 12]. It should be noted that, after the groundbreaking impact of graphene, the scientific community is actively exploring other two-dimensional semiconductors "beyond graphene", such as phosphorene and Bi_2Se_3 [13, 14], for their promising applications capabilities, ranging from nanoelectronics, nanophotonics and nanomedicine [15, 16].

A reconfigurable antenna is designed in a manner that it is possible to manually or automatically change its resonant frequency, operational bandwidth, radiation pattern. This is most commonly done with electromechanical systems (MEMS or NEMS) [17, 18], electrical RF switches [19, 20], diode-based technology such as the P-type Insulator N-type diode (PIN diode) [21, 22], varactors [23], or tunable

* Corresponding author: Aymen Hlali (Hlaliaymen683@gmail.com).
The authors are with the Unit of Mechatronic Systems and Signals, National Engineering School of Carthage, University of Carthage, Tunis, Tunisia.

materials [24], via applying a mechanical, electrical, magnetic, light or thermal bias [25]. The most significant merit is that the properties of graphene-based antennas can be easily controlled using electric field effect in the THz frequency. Thus, the tunability of graphene has been widely used for small reconfigurable devices in the terahertz regime.

The paper is structured as follows. Section 2 will introduce the conductivity of graphene and a brief introduction to the wave concept iterative process method, including the development of the new operator diffraction of the graphene in the spatial domain. Then, Section 4 will define the proposed antenna designs. Afterwards, the simulation results are presented and discussed in Section 5. Finally, Section 6 will finish the paper with key conclusions.

2. FORMULATION

2.1. Modeling of Graphene

Graphene is modeled as a sheet conductor whose surface conductivity consists of two terms intraband conductivity and interband conductivity [26]. However, in the Terahertz-frequency band, the first term dominates the value of total conductivity whereas the second term has no significant effect on the overall surface conductivity within this band [27]. Hence, the conductivity of graphene can be expressed by using the only intraband term, which can be evaluated as

$$\sigma_{\text{intra}} = -j \frac{e^2 K_B T}{\pi \hbar^2 (\omega - j 2\Gamma)} \left[\frac{\mu_c}{K_B T} + 2 \ln \left(e^{-\frac{\mu_c}{K_B T}} + 1 \right) \right] \tag{1}$$

and the interband conductivity is

$$\sigma_{\text{inter}} \simeq -j \frac{e^2}{4\pi\hbar} \ln \left[\frac{2|\mu_c| - (\omega - j 2\Gamma)\hbar}{2|\mu_c| + (\omega - j 2\Gamma)\hbar} \right] \tag{2}$$

where K_B is the Boltzmann constant, $\hbar$ the reduced Planck's constant, e the electron charge, ω the angular frequency, Γ the scattering rate, T the temperature, and μ_c the chemical potential. The intraband conductivity is a complex quantity that can be expressed by $\sigma = \sigma_r + j\sigma_i$, where σ_r and σ_i are respectively the real and imaginary parts of the conductivity.

The variations of the real and imaginary parts of the intraband conductivity versus frequency for several different chemical potentials μ_c for 0 to 0.4 eV with $T = 300$ K and $\tau = 10^{-13}$ s are shown in Figs. 1 and 2.
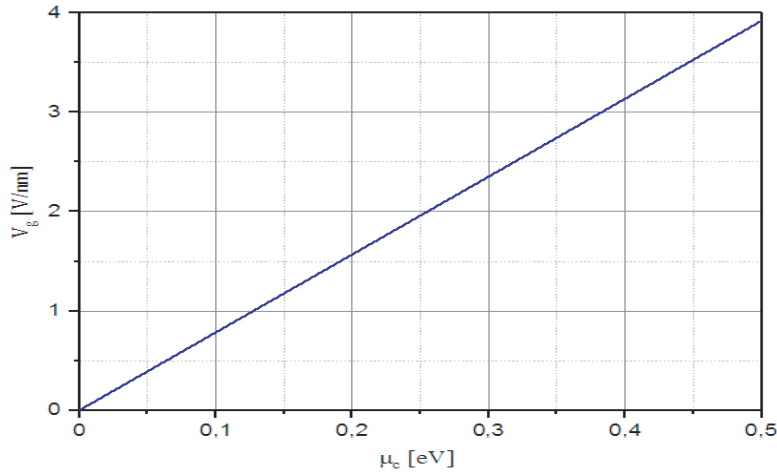
From these two figures, we can see the effect of changing chemical potential on the conductivity; it depends on the carrier density, which can be controlled by a bias voltage. The relation between the
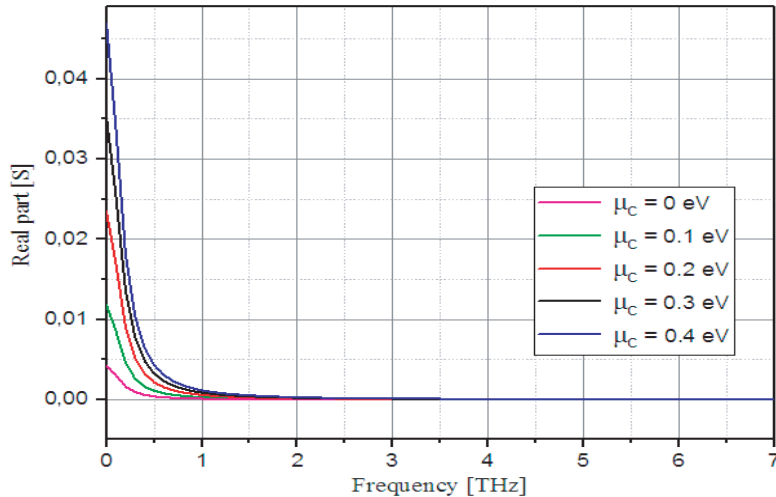
Figure 1. Real part of graphene's conductivity.
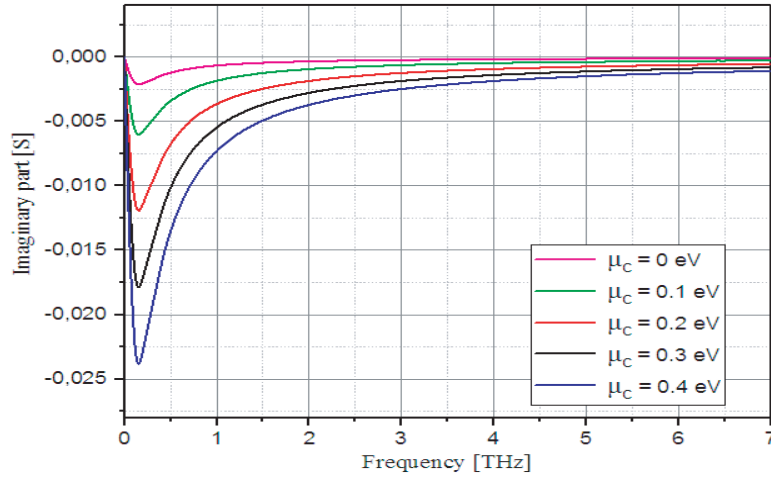
Figure 2. Imaginary part of graphene's conductivity.

Figure 3. The relationship between bias voltage and chemical potential.

bias voltage and chemical potential in graphene obtained from Eq. (3) is shown in Fig. 3 [28].

$$V_g = \frac{e\mu_c{}^2 h}{\pi \hbar^2 V_f^2 \varepsilon_0 \varepsilon_r} \tag{3}$$

where V_g is the applied voltage on graphene, h the thickness of the substrate, ε_r the substrate permittivity, and V_f the Fermi velocity in graphene.

We observe that the potential chemical increases with an increase in bias voltage, hence the increase of the conductivity. Therefore, reconfigurable characteristics can be obtained.

2.2. Modeling of Graphene in the WCIP Method

Analysis of planar structures with our electromagnetic method called wave concept iterative method WCIP has been described in detail in various articles [29, 30]. Therefore, a brief overview of the WCIP method is presented here. It is based on the Wave Concept, which is introduced by writing the incident and reflected waves as a function of the transverse electric and magnetic fields. It leads to the following set of equations

$$\vec{A}_i = \frac{1}{2\sqrt{Z_{0i}}} \left(\vec{E}_i + Z_{0i} \vec{J}_i \right) \tag{4}$$

$$\vec{B}_i = \frac{1}{2\sqrt{Z_{0i}}} \left(\vec{E}_i - Z_{0i}\vec{J}_i \right) \tag{5}$$

where i indicates medium 1 or 2 corresponding to a given interface. Z_{0i} is the characteristic impedance of the same medium i, and $\vec{J}_i$ the surface current density vector is given as

$$\vec{J}_i = \vec{H}_i \times \vec{n}_i \tag{6}$$

with $\vec{n}_i$ being the normal vector to the interface. Thus, the tangential electric and magnetic fields can be calculated from

$$\vec{E}_i = \sqrt{Z_{0i}} \left(\vec{A}_i + \vec{B}_i \right) \tag{7}$$

$$\vec{J}_i = \frac{1}{\sqrt{Z_{0i}}} \left(\vec{A}_i - \vec{B}_i \right) \tag{8}$$

After process convergence the scatring matrix S_{ij} can be obtained by the following equation

$$[S] = \frac{1 - [Y]}{1 + [Y]} \tag{9}$$

where $[Y]$ is the matrix admittance.

In order to implement the model of graphene sheet in the WCIP method, the boundary conditions at the sheet can be represented as [27]

$$\vec{n} \times \left(\vec{H}_1 - \vec{H}_2 \right) = \vec{J}_s \tag{10a}$$

$$= \sigma \vec{E} \tag{10b}$$

where $\vec{n}$ denotes the unit vector normal to the graphene sheet; $\vec{H}_1$ and $\vec{H}_2$ are the magnetic fields at two sides of the sheet; $\vec{J}_s$ is the surface current density; $\vec{E}$ is the electric field. Generally, modeling by the WCIP method consists of converting the magnetic field $\vec{H}$ by the current density $\vec{J}$, and we can write

$$\vec{n} \times \left(\vec{H}_1 - \vec{H}_2 \right) = \vec{J}_1 + \vec{J}_2 \tag{11}$$

The electric field may be written as

$$\vec{E} = \vec{E}_1 = \vec{E}_2 \tag{12}$$

By replacing Equations (8) and (9) in Equation (7), we obtain the following equations

$$\vec{J}_1 + \vec{J}_2 = \sigma \vec{E}_1 \tag{13}$$
$$\vec{J}_1 + \vec{J}_2 = \sigma \vec{E}_2 \tag{14}$$

In terms of waves and after a mathematical resolution, these equations are finalized at

$$\begin{pmatrix} \vec{B}_1 \\ \vec{B}_2 \end{pmatrix} = \begin{pmatrix} S_{11} & S_{12} \\ S_{21} & S_{22} \end{pmatrix} \begin{pmatrix} \vec{A}_1 \\ \vec{A}_2 \end{pmatrix} \tag{15}$$

where S_{ij} are defined by

$$S_{11} = \frac{Z_{02} - Z_{01} - \sigma Z_{02}Z_{01}}{Z_{02} + Z_{01} + \sigma Z_{02}Z_{01}} \tag{16}$$

$$S_{12} = \frac{2Z_{02}\sqrt{Z_{01}}}{\sqrt{Z_{02}}(Z_{02} + Z_{01} + \sigma Z_{02}Z_{01})} \tag{17}$$

$$S_{21} = \frac{2Z_{01}\sqrt{Z_{02}}}{\sqrt{Z_{02}}(Z_{02} + Z_{01} + \sigma Z_{02}Z_{01})} \tag{18}$$

$$S_{22} = -\frac{Z_{02} - Z_{01} + \sigma Z_{02}Z_{01}}{Z_{02} + Z_{01} + \sigma Z_{02}Z_{01}} \tag{19}$$

The interface in which the circuit is defined is divided into small sub-domains, and the interface contains four sub-domains (dielectric, metal, graphene and source). By using the boundary condition in each region [31, 32], it is possible to define the overall diffraction operator, which binds the incident waves to the reflected waves in the spatial domain:

$$\Gamma = \Gamma_G + \Gamma_m + \Gamma_d + \Gamma_s = \begin{pmatrix} \Gamma_{11} & \Gamma_{12} \\ \Gamma_{21} & \Gamma_{22} \end{pmatrix} \tag{20}$$

where $\Gamma_G, \Gamma_m, \Gamma_d$ and Γ_s are respectively the graphene, metal, dielectric and source domain diffraction operators.

with Γ_{ij} is expressed by

$$\Gamma_{11} = \left[-H_m + \frac{Z_{02} - Z_{01} - \sigma Z_{02} Z_{01}}{Z_{02} + Z_{01} + \sigma Z_{02} Z_{01}} H_g + \frac{1 - n^2}{1 + n^2} H_d + \frac{-1 + n_1 - n_2}{1 + n_1 + n_2} H_s \right]$$

$$\Gamma_{12} = \left[\frac{2 Z_{02} \sqrt{Z_{01}}}{\sqrt{Z_{02}}(Z_{02} + Z_{01} + \sigma Z_{02} Z_{01})} H_g + \frac{2n}{1 + n^2} H_d + \frac{2m}{1 + n_1 + n_2} H_s \right]$$

$$\Gamma_{21} = \left[\frac{2 Z_{01} \sqrt{Z_{02}}}{\sqrt{Z_{02}}(Z_{02} + Z_{01} + \sigma Z_{02} Z_{01})} H_g + \frac{2n}{1 + n^2} H_d + \frac{2m}{1 + n_1 + n_2} H_s \right]$$

$$\Gamma_{22} = \left[-H_m - \frac{Z_{02} - Z_{01} + \sigma Z_{02} Z_{01}}{Z_{02} + Z_{01} + \sigma Z_{02} Z_{01}} H_g - \frac{1 - n^2}{1 + n^2} H_d + \frac{-1 - n_1 + n_2}{1 + n_1 + n_2} H_s \right]$$

where $n = \sqrt{\frac{Z_{01}}{Z_{02}}}$, $m = \frac{Z_0}{\sqrt{Z_{01} Z_{02}}}$, $n_1 = \frac{Z_0}{Z_{01}}$ and $n_2 = \frac{Z_0}{Z_{02}}$.

3. DESIGN OF THE PROPOSED ANTENNA

In this paper, the design of the dual-band reconfigurable graphene antenna started with a comparative investigation of no-doped graphene and metal. Figures 4(a), (b), (c) and (d) show the front view of the proposed antenna, with four different configurations, chosen for their simplicity and ease of fabrication.
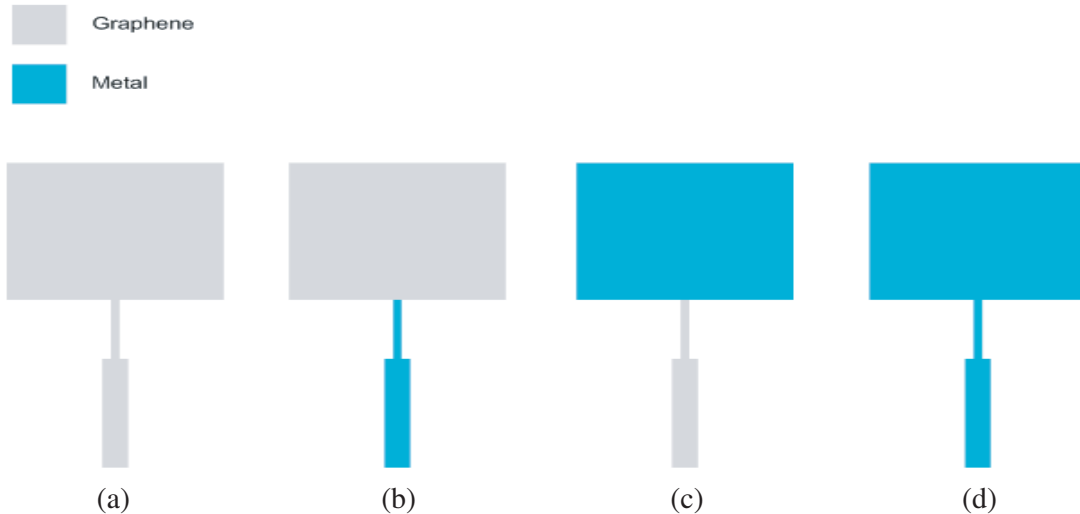

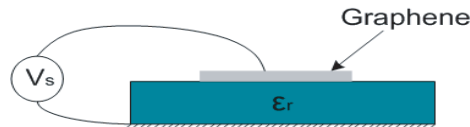Figure 4. Structure of the proposed antenna.

Figure 5. 3D view of the proposed antenna.

All the antennas consist of a conducting patch and a feeding line and are printed on a Duroid dielectric substrate with relative permittivity 2.2 and height 3 μm.

Figure 5 shows the 3D view of our proposed dual-band reconfigurable graphene antenna controlled by the bias voltage. Table 1 gives the optimized dimensional parameters of the antenna.

**Table 1.** Parameters of the proposed antenna.

| Parameters	Value (μm)
Substrate length and width	103×97
Substrate thickness	3
Substrate dielectric constant (Duroid, ϵ_r)	2.2
Side length and width of square patch	23.33×28.79
Length of feed	23.33
Width of feed	4.54
Length of $\lambda/4$ transformer	14.48
Width of $\lambda/4$ transformer	1.51

4. NUMERICAL RESULTS AND DISCUSSIONS

In this section, we perform a detailed discussion about the response of the dual-band reconfigurable graphene antenna. The formulation developed in Section 2 is implemented in FORTRAN code. The main target is to prove the applicability of the formulation of graphene in WCIP in the THz range. In fact, we present different numerical results for the four configurations shown in the previous section.

### 4.1. Comparative Investigation of No-Doped Graphene and Metal

In order to compare the performance of no-doped graphene and metal for the proposed nano-patch antenna in the terahertz region, we simulated the structures presented in the previous section. For this purpose, we started with the convergence study and boundary conditions. The convergence of the iterative process is examined for the four configurations. Figure 6 shows the variation of the return loss as a function of the number of iterations at the resonant frequencies.
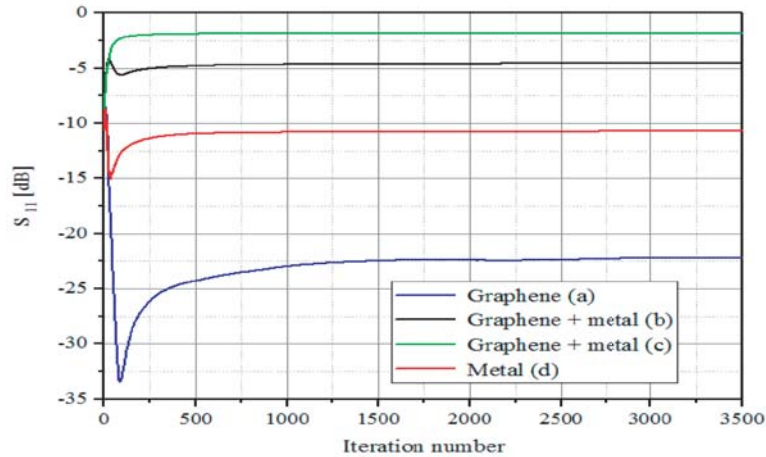
Figure 6. Convergence of the return loss S_{11} versus the number of iterations.
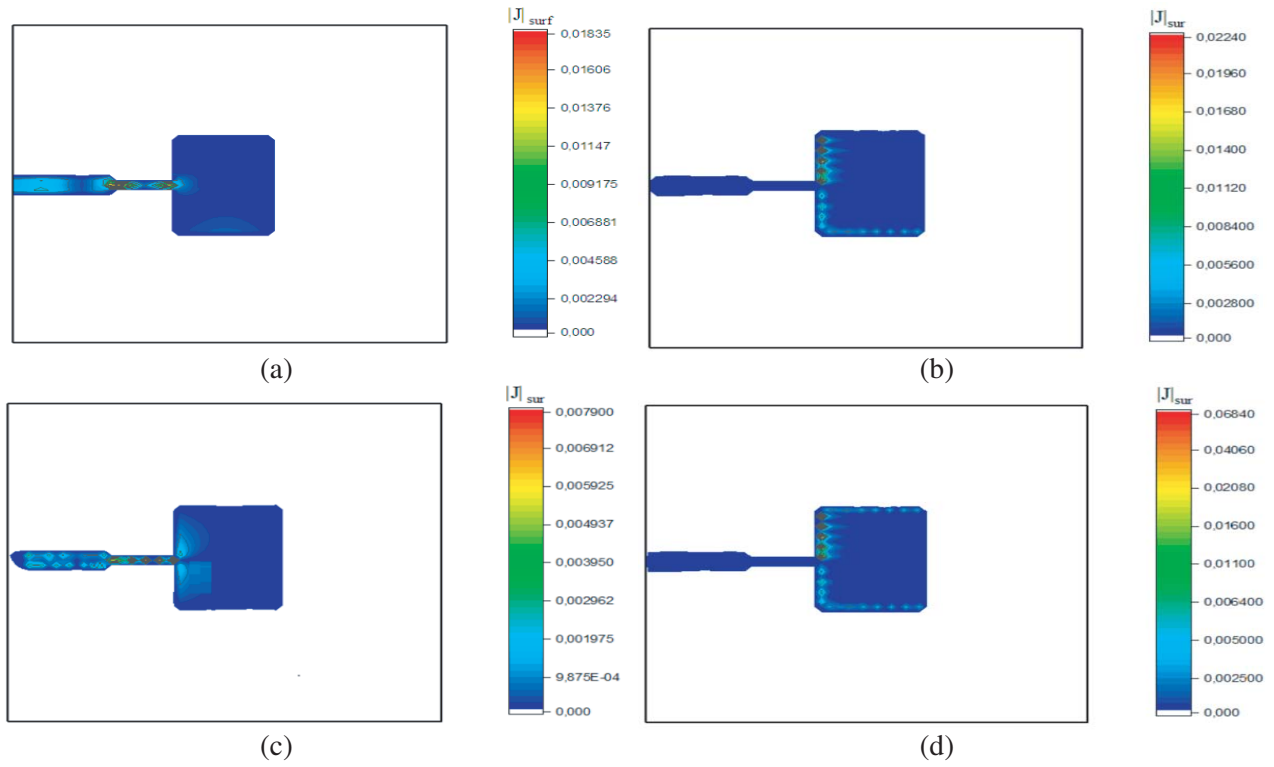
Figure 7. Distribution of the current density of the interface for the four configurations. (a) Graphene. (b) Graphene + metal. (c) Graphene + metal. (d) Metal.
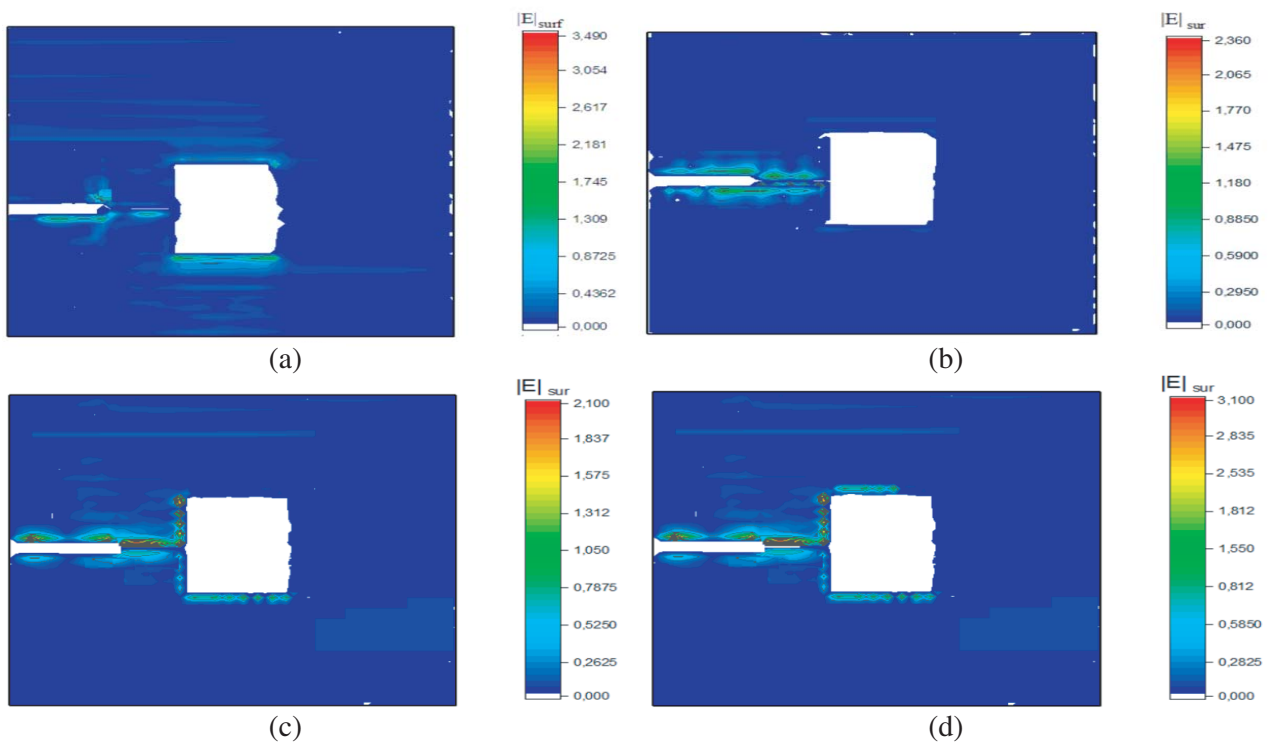

Figure 8. Distribution of the electric field of the interface for the four configurations. (a) Graphene. (b) Graphene + metal. (c) Graphene + metal. (d) Metal.

We find that the convergence of the graphene-based antenna (a) is obtained from 1500 iterations and 700 iterations for the other structures. Figures 7 and 8 illustrate the distribution of currents and fields for each structure.

According to these figures, we notice that the electric field and current density satisfy the boundary conditions, since the density of the current is defined only on the graphene and metal, and zero on the dielectric. The electric field is zero on graphene and metal, and different from zero on the dielectric.

To validate the results obtained by the formulation of the graphene developed by the WCIP method, a comparison with the results obtained by the CST simulator was realized. Figure 9 shows the graph that compares the return loss of the no-doped graphene-based antenna (a) obtained through the WCIP method and CST simulator.
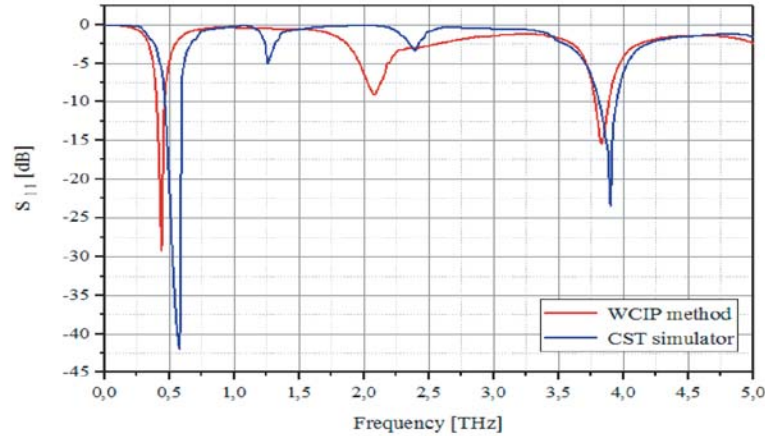
Figure 9. Comparative curves of the return loss S_{11} of no-doped graphene-based antenna (a) versus frequency.

We notice that the simulated result obtained by WCIP is very close to that obtained by the CST simulator. This also validates the formulation of the graphene developed by the WCIP method.

Figure 10 illustrates the variation of the reflection coefficient for the four studied configurations mentioned in the previous section.
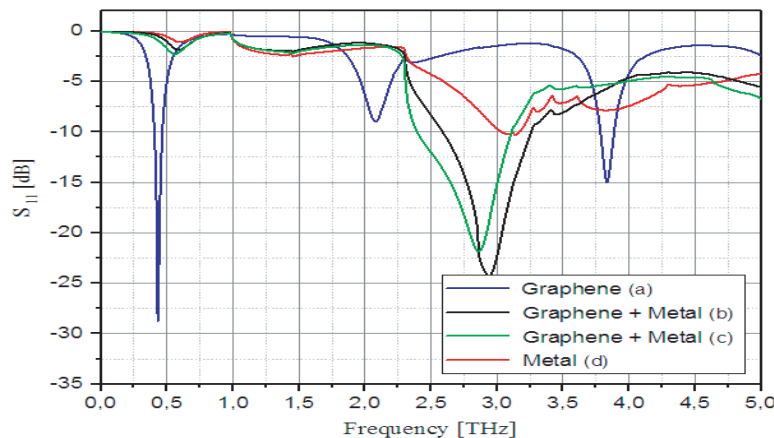

Figure 10. Performance comparison of the return loss versus frequency for the four configurations.

It shows that the reflection coefficient of the metal-based antenna (d) is badly adapted compared to the graphene-based antenna (a). It is evident, since the metal is not usable in the THz regime. Besides that, by the implementation of the graphene in hybrid structures (b) and (c), the antenna performance

is enhanced drastically compared to the metal-based antenna in terms of the reflection coefficient. In this case, the return loss is reduced from -10 to -24 dB.

According to Figures 10 and 11, graphene-based antenna (a) showed better adaptation. For this, we continue our study with this antenna.
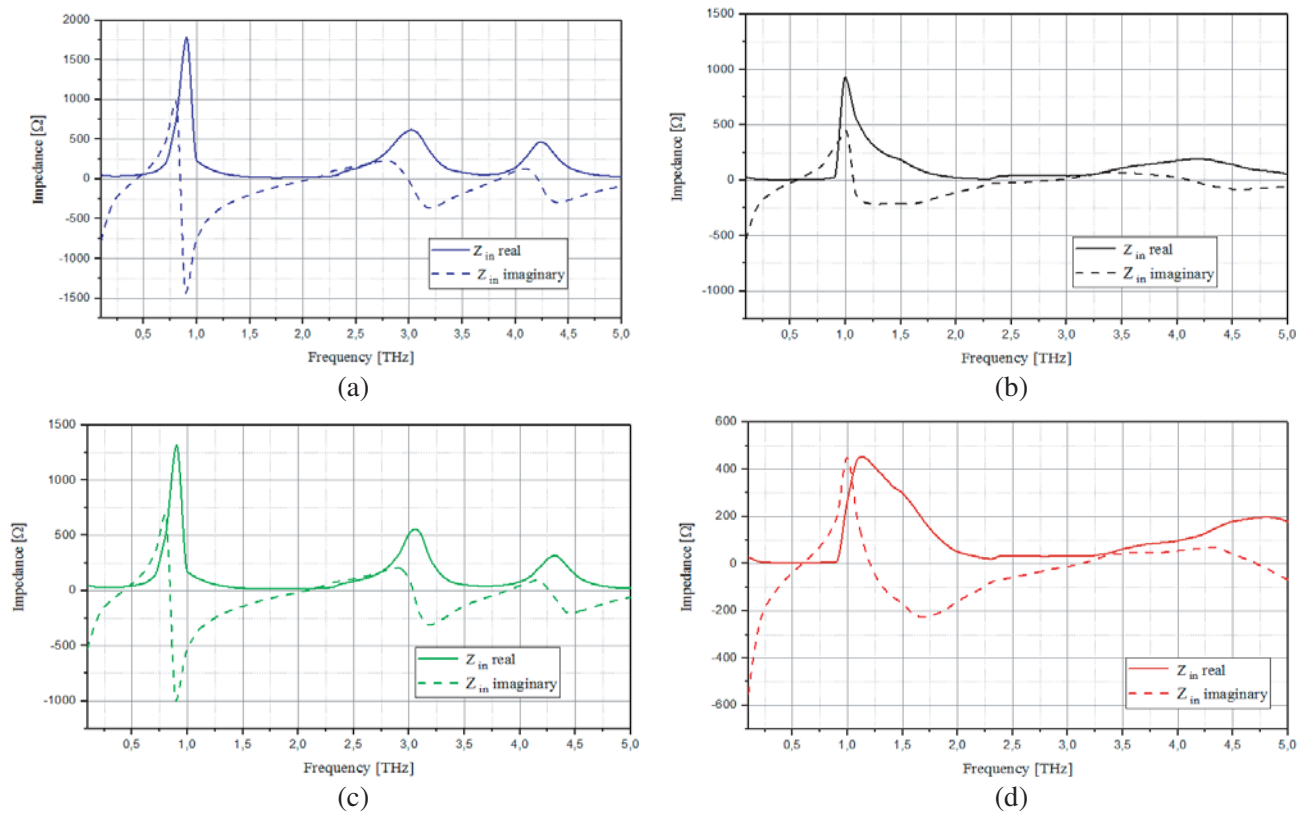
Figure 11. Real and imaginary parts of input impedance for the four configurations. (a) Graphene. (b) Graphene + metal. (c) Graphene + metal. (d) Metal.
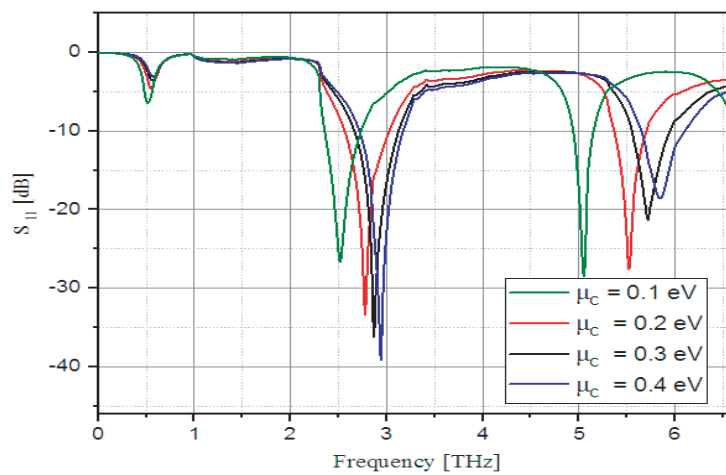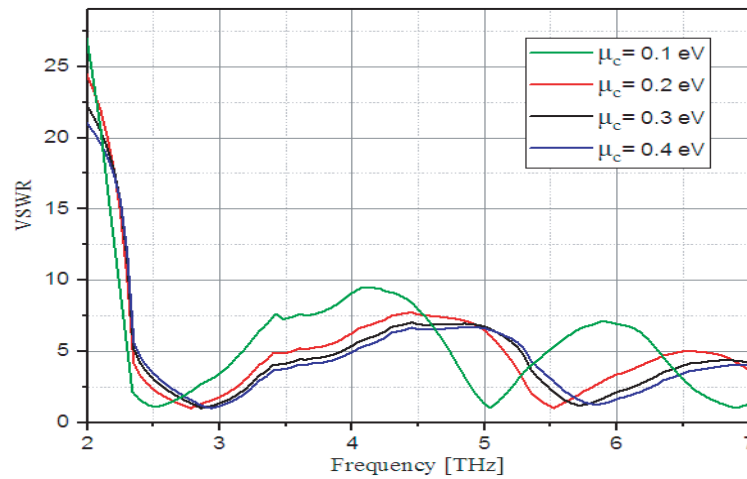

Figure 12. Return loss versus frequency for different chemical potential.

4.2. Performance Analysis of Reconfigurable Graphene Antenna

Here, the performance of the graphene-based antenna (a) was evaluated. The simulation results obtained for return loss characteristics over the considered 0.1–0.4 eV range of chemical potential are shown in Figure 12. Here the temperature is assumed 300 K, and the relaxation time is selected as 0.1 ps.

It can be seen that it exhibits two resonant frequency bands over the whole frequency range, namely 2.5–2.95 and 5.06–5.84 THz. It is exciting to note that the return loss decreases by increasing the chemical potential in the first resonance band and the reverse in the second band. The resonant frequency shift observed is irregular and somewhat linear.

Figure 13 shows the values obtained for voltage standing wave ratio (VSWR) for its potential chemical values from 0.1 to 0.4 eV at their respective resonating frequencies.

Figure 13. VSWR versus frequency for different chemical potential.

Another parameter is the relaxation time of the graphene, which is studied in Figure 14, and the temperature effect in graphene is considered at Figure 15.
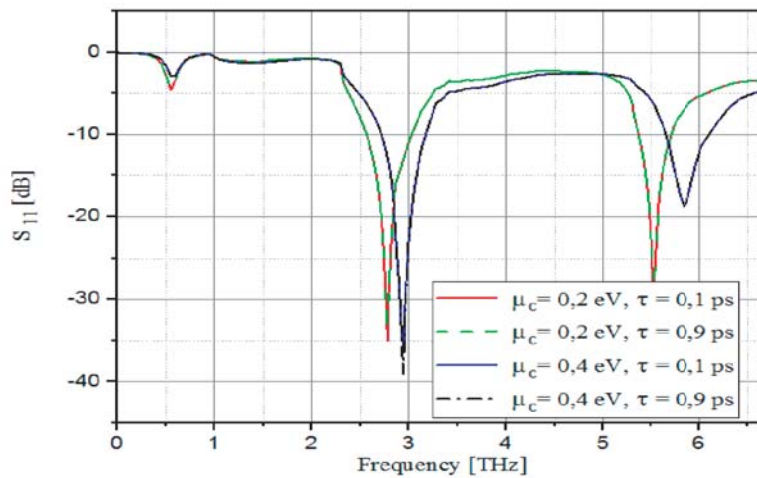
Figure 14. Return loss versus frequency for various graphene with various relaxation times.

As shown here, to study the relaxation time effect, we have considered two relaxation times of 0.1 and 0.9 pS for two different chemical potentials of the 0.2 and 0.4 eV. The results show that the
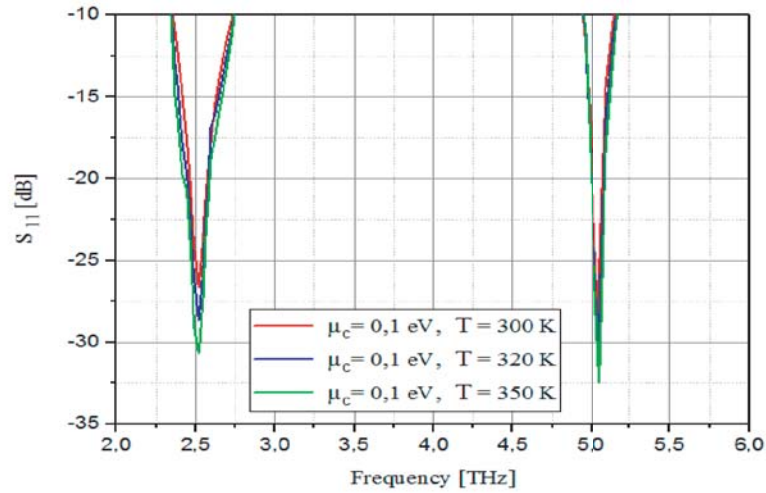
Figure 15. Return loss versus frequency for various graphene with various temperatures.
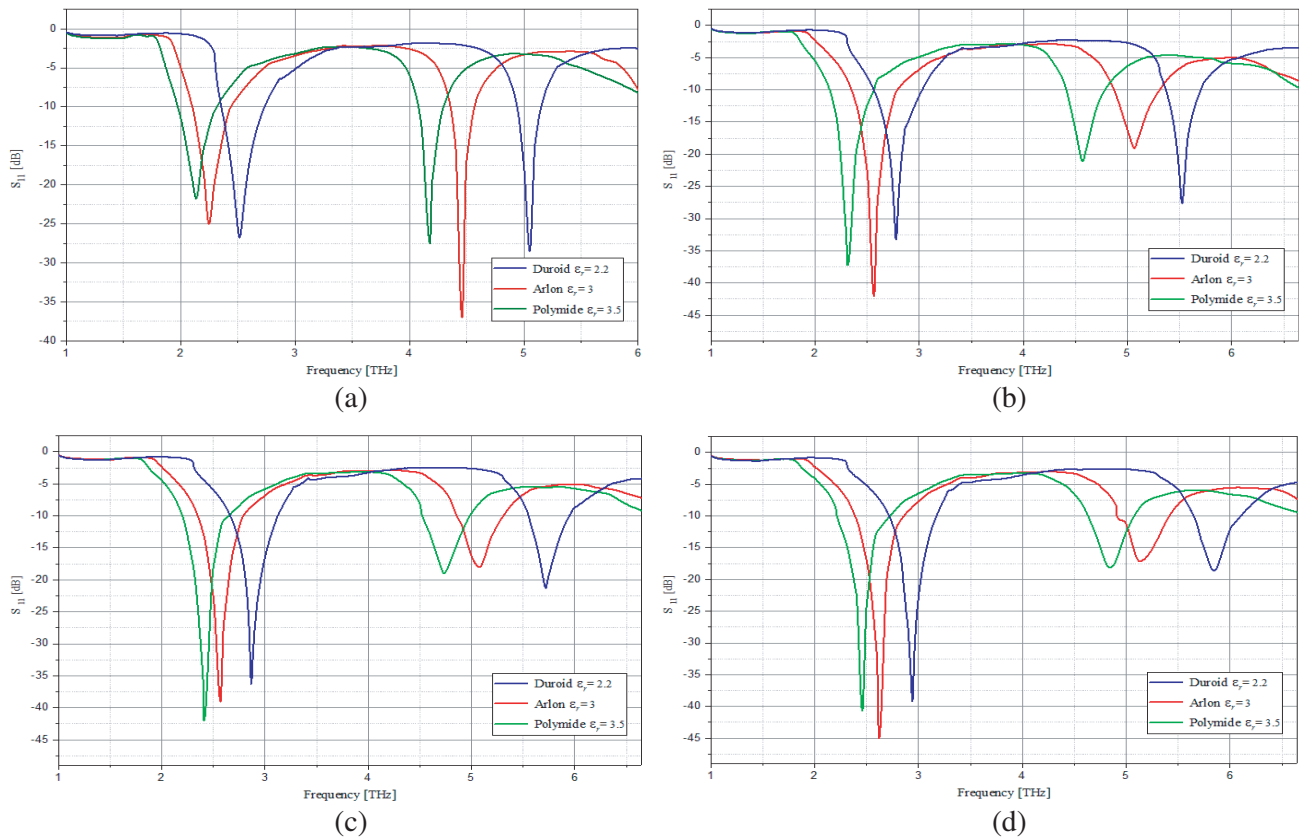
Figure 16. Return loss versus frequency for various substrates materials. (a) $\mu_c = 0.1$. (b) $\mu_c = 0.2$. (c) $\mu_c = 0.3$. (d) $\mu_c = 0.4$.

relaxation time does not have any effect on this antenna.

On the other hand, the graphene temperature effect has been investigated, and the result shows that by increasing the temperature we have a small change in the reflection value, which reaches 11.11% in the first resonant frequency and 16.01% in the second.

Next, the performance comparison of the proposed graphene-based dual-band antenna for various substrate materials is investigated. It can be observed in Figure 16 that return loss values for different materials reach their peak values below $-10\,\mathrm{dB}$ at resonating frequency around 2500–2950 and 4460–5844 GHz for all the selected substrates. The best conditions are achieved for Arlon with $0.4\,\mathrm{eV}$ for the chemical potential with return loss reaching the maximum value of $-44.98\,\mathrm{dB}$.

For various substrate materials, the bandwidth achieved is in the range of 210–495 GHz at different resonant frequencies as depicted in Table 2. It can be seen that the maximum bandwidth of 495 GHz is obtained for the Polyimide substrate with $\mu_c = 0.4\,\mathrm{eV}$.

Table 2. Performance comparison of the proposed antenna for various substrate materials.

Substrate parameters	Chemical potential [eV]	$\mathrm{Fr}_{1,2}$ [GHz]	Return $\mathrm{Loss}_{1,2}$ [dB]	$\mathrm{Bandwidth}_{1,2}$ [GHz]	$\mathrm{VSWR}_{1,2}$
Duroid $\epsilon_r = 2.2$	$\mu_c = 0.1$	2500, 5061	$-26.57, -28.52$	386, 216	1.1, 1.08
	$\mu_c = 0.2$	2783, 5537	$-33.33, -27.67$	457, 341	1.04, 1.09
	$\mu_c = 0.3$	2861, 5729	$-36.12, -21.30$	467, 395	1.03, 1.19
	$\mu_c = 0.4$	2950, 5844	$-39.18, -18.47$	476, 463	1.02, 1.27
Arlon $\epsilon_r = 3$	$\mu_c = 0.1$	2250, 4460	$-24.41, -36.93$	340, 210	1.12, 1.34
	$\mu_c = 0.2$	2565, 5060	$-42.05, -18.61$	440, 425	1.01, 1.26
	$\mu_c = 0.3$	2570, 5070	$-38.34, -17.98$	450, 437	1.02, 1.29
	$\mu_c = 0.4$	2620, 5130	$-44.98, -16.85$	460, 448	1.01, 1.34
Polyimide $\epsilon_r = 3.5$	$\mu_c = 0.1$	2130, 4180	$-21, 61, -27.56$	325, 225	1.18, 1.09
	$\mu_c = 0.2$	2310, 4560	$-37.22, -20.56$	425, 387	1.02, 1.20
	$\mu_c = 0.3$	2410, 4740	$-42.01, -19.03$	450, 435	1.01, 1.25
	$\mu_c = 0.4$	2460, 4850	$-40.63, -17.81$	495, 445	1.01, 1.29

A second important observation is that as the value of potential chemical increases, the bandwidth should increase.

5. CONCLUSION

In this paper we analyze the performance of using graphene in frequency reconfigurable antennas in the THz regime for medical and imaging applications. The results clearly show the antenna can be tuned via changing the chemical potential. So, the bias electric field is a significant factor for the reconfigurable THz antenna. Furthermore, we have investigated the effect of additional parameters such as temperature and relaxation time. Fabrication of the prototype and experimental study of the proposed structure are needed in the future to validate our intended results.

REFERENCES

1. Kyungho, H., T. K. Nguyen, I. Park, and H. Han, "Terahertz Yagi-Uda antenna for high input resistance," *J. Infrared Millim. Terahertz Waves*, Vol. 31, 441–451, 2010.
2. Kazemi, A. H. and A. Mokhtari, "Graphene-based patch antenna tunable in the three atmospheric windows," *Inter. J. Light Electron Opt.*, Vol. 142, 475–482, 2017.
3. Ramezan, A. S. and B. Z. Ferdows, "Metamaterial Fabry-Perot cavity implementation for gain and bandwidth enhancement of THz dipole antenna," *Inter. J. Light Electron Opt.*, Vol. 127, 5181–5185, 2016.
4. Sirisha, M. and M. Arun, "Dual-band reconfigurable graphene-based patch antenna in terahertz band for wireless network-on-chip applications," *IET Micr., A. & Prop.*, Vol. 11, 2104–2108, 2017.

5. Mir, M. S. and A. S. Ramazan, "Antenna gain enhancement by using metamaterial radome at THz band with reconfigurable characteristics based on graphene load," *J. Opt. Quant. Elec.*, Vol. 221, 1–13, 2017.

6. Alexander, I. M., Y. Bin, M. G. Stephen, W. Michael, and S. D. Robert, "Terahertz spectroscopy: A powerful new tool for the chemical sciences?," *Chem. Soc. Rev.*, Vol. 41, 2072–2082, 2012.

7. Nikita, V. Ch., E. F. Maxim, P. Sergey, et al., "Wide-aperture aspherical lens for high-resolution terahertz imaging," *Rev. Sci. Instrum.*, Vol. 88, 1–6, 2017.

8. Dhillon, S. S., M. S. Vitiello, E. H. Linfield, A. G. Davies, M. C. Hoffmann, et al., "The 2017 terahertz science and technology roadmap," *J. Phy. D: Appl. Phy.*, Vol. 50, No. 4, 1064–1076, 2017.

9. Novoselov, K. S., V. I. Colombo, P. R. Gellert, M. G. Schwab, and K. Kim, "A roadmap for graphene," *Nature*, Vol. 490, No. 7419, 192–200, 2012.

10. Novoselov, K. S., A. K. Geim, S. V. Morozov, D. Jiang, Y. Zhang, S. V. Dubonos, I. V. Grigorieva, and A. A. Firsov, "Electric field effect in atomically thin carbon films," *Science*, Vol. 306, No. 10, 666–669, 2004.

11. Antonio P. and Ch. Gennaro, "Plasmon modes in graphene: Status and prospect," *The Royal Society of Chemistry*, Vol. 6, 10927–10940, 2014.

12. Tamagnone, M., J. S. Gymez-Dıaz, J. R. Mosig, and J. Perruisseau-Carrier, "Reconfigurable terahertz plasmonic antenna concept using a graphene stack," *Appl. Phys. Lett.*, Vol. 101, 214101–214104, 2012.

13. Leonardo, V., H. Jin, C. Dominique, P. Antonio, K. Wojciech, and S. V. Miriam, "Efficient terahertz detection in black-phosphorus nano-transistors with selective and controllable plasma-wave, bolometric and thermoelectric response," *Scientific Reports*, Vol. 6, 1–23, 2016.

14. Leonardo, V., C. Dominique, P. Antonio, K. Konstantin, A. Ziya, B. Mahammad, et al., "Plasma-wave terahertz detection mediated by topological insulators surface states," *Nano Letters*, Vol. 16, 1–18, 2016.

15. Tang, W., A. Politano, C. Guo, W. Guo, C. Liu, and L. Wang, X. Chen, and W. Lu, "Ultrasensitive room-temperature terahertz direct detection based on a bismuth selenide topological insulator," *Adv. Funct. Mater.*, 1–9, 2018.

16. Amit, A., S. V. Miriam, V. Leonardo, C. Anna, and P. Antonio, "Plasmonics with two-dimensional semiconductors: From basic research to technological applications," *Nanoscale*, Vol. 10, 1–11, 2018.

17. Jung, C. W., M. J. Lee, G. P. Li, and F. D. Flaviis, "Re-configurable scan-beam single-arm spiral antenna integrated with RFMEMS switches," *IEEE Trans. Antennas Propag.*, Vol. 54, No. 2, 455–463, 2006.

18. Cetiner, B. A., G. R. Crusats, L. Jofre, and N. Biyikli, "RF MEMS integrated frequency reconfigurable annular slot antenna," *Journal Title Abbreviation*, Vol. 58, No. 3, 626–632, 2010.

19. Pringle, L. N., et al., "A reconfigurable aperture antenna based on switched links between electrically small metallic patches," *IEEE Trans. Antennas Propag.*, Vol. 52, No. 6, 1434–1445, 2004.

20. Aboufoul, T., A. Alomainy, and C. Parini, "Reconfiguring UWB monopole antenna for cognitive radio applications using GaAs FET switches," *IEEE Antennas Wireless Propag. Lett.*, Vol. 11, 392–394, 2012.

21. Peroulis, D., K. Sarabandi, and L. P. B. Katehi, "Design of reconfigurable slot antennas," *IEEE Trans. Antennas Propag.*, Vol. 53, No. 2, 645–654, 2005.

22. Lee, S. W. and Y. Sung, "Compact frequency reconfigurable antenna for lte/wwan mobile handset applications," *IEEE Trans. Antennas Propag.*, Vol. 63, No. 10, 4572–4577, 2015.

23. Khidre, A., F. Yang, and A. Z. Elsherbeni, "A patch antenna with a varactor-loaded slot for reconfigurable dual-band operation," *IEEE Trans. Antennas Propag.*, Vol. 63, No. 2, 755–760, 2015.

24. Haupt, R. L., "Re-configurable patch with switchable conductive edges," *Microw. Opt. Technol. Lett.*, Vol. 51, No. 7, 1757–1760, 2009.

25. Haupt, R. L. and M. Lanagan, "Re-configurable antennas," *IEEE Antennas Propag. Mag.*, Vol. 55, No. 1, 49–61, 2013.

26. Hanson, G. W., "Dyadic Green's functions and guided surface waves for a surface conductivity model of graphene," *J. Ap. Phys.*, Vol. 103, 064302–064302, 2008.

27. Cao, Y. S., L. J. Jiang, and A. E. Ruehli, "An equivalent circuit model for graphene-based terahertz antenna using the PEEC method," *IEEE Trans. Antennas Prop.*, Vol. 64, 1385–1393, 2016.

28. Gatte, M. T., P. J. Soh, H. A. Rahim, R. B. Ahmad, and F. Malek, "The performance improvement of THz antenna via modeling and characterization of doped graphene," *Progress In Electromagnetics Research M*, Vol. 49, 21–31, 2016.

29. Houaneb, Z., H. Zairi, A. Gharsallah, and H. Baudrand, "A new wave concept iterative method in cylindrical coordinates for modeling of circular planar circuits," *Eighth Inter. Multi-Conference on Systems, Signals Devices*, 1–7, 2011.

30. Hajlaoui, A., H. Trabelsi, and H. Baudrand, "Periodic planar multilayered substrates analysis using wave concept iterative process," *J. Elec. Analy. Appl.*, Vol. 3, 118–128, 2012.

31. Zairi, H., A. Gharsallah, A. Gharbi, and H. Baudrand, "Analysis of planar circuits using a multigrid iterative method," *IEE Proc. Micro., Antennas and Prop.*, Vol. 153, 109–162, 2006.

32. Tellache, M., Y. Lamhene, B. Haraoubia, and H. Baudrand, "Application of wave concept iterative process to analys emicrowave planar circuits," *Inter. J. App. Electr. and Mechanics*, Vol. 29, 131–143, 2009.